Defence Technology 33 (2024) 180–185

Contents lists available at ScienceDirect

Defence Technology

journal homepage: www.keaipublishing.com/en/journals/defence-technology

Construction of smart propellant with multi-morphologies

Weitao Yang [a, *], Yuchen Gao [a], Rui Hu [a], Manman Li [a], Fengqi Zhao [a], He Jiang [b], Xuan Zhang [b, **]

[a] Xi'an Modern Chemistry Research Institute, Xi'an, 710065, China
[b] Northwestern Polytechnical University, Xi'an, 710072, China

ARTICLE INFO

Article history:
Received 25 April 2023
Received in revised form
8 June 2023
Accepted 27 June 2023
Available online 29 June 2023

Keywords:
Smart material
Gun propellants
Multi-morphologies
Self-regulation

ABSTRACT

Smart materials, which exhibit shape memory behavior in response to external stimuli, have shown great potential for use in biomedical applications. In this study, an energetic composite was fabricated using a UV-assisted DIW 3D printing technique and a shape memory material (SMP) as the binder. This composite has the ability to reduce the impact of external factors and adjust gun propellant combustion behavior. The composition and 3D printing process were delineated, while the internal structure and shape memory performance of the composite material were studied. The energetic SMP composite exhibits an angle of reversal of 18 s at 70°, with a maximum elongation typically reaching up to 280% of the original length and a recovery length of approximately 105% during ten cycles. Additionally, thermal decomposition and combustion behavior were also demonstrated for the energetic SMP composite.

1. Introduction

A propellant is a chemical substance that is used to produce energy or pressurized gas, which is subsequently utilized to create fluid movement or generate propulsion for vehicles, projectiles, or other objects. Solid propellants may be used in guns, mortars, rockets, explosive ordnance disposal units, bomb release cartridges, ejection cartridges, fireworks and other applications. All propellants have a temperature coefficient which results in higher maximum pressure and muzzle velocity at high temperatures compared to lower temperatures when used in a gun [1,2]. The temperature coefficient of the combustion rate of the propellant is the response of the burn rate change with the initial propellant temperature, and several methods have been used to decrease the temperature coefficient such as deterred or surface-coated propellants [3,4].

In traditional knowledge, the geometry and morphology of solid propellant charges are fixed once they have been built. The propellants lack the ability to self-adjust and self-regulate. Once off the production line, their gas generation behavior is set, meaning that their interior ballistic performance is also set. Propellants burn faster at higher temperatures than at lower ones, resulting in a temperature coefficient of interior ballistic performance [5]. As the gas generation rate is proportional to the product of burning rate and surface area, it may be possible to use a smart material devised to affect the combustion surface area of the propellant grains.

In the past decade, UV-assisted DIW 3D printing has undergone significant development and technical difficulties have been overcome, including the use of energetic photocurable binders, formulations with high energy content, and the construction of three-dimensional energetic objects [6–8]. With growing interest in additive manufacturing and advances in materials science, there is a desire to utilize "smart" materials for solid propellants [9]. As the temperature of these propellants changes, so too does the shape of the smart material, leading to an adjustable surface area and gas generation behavior.

Shape memory polymers (SMPs) are a type of intelligent material that can be programmed to retain a temporary shape and recover their original shape under external stimuli, such as temperature, light, electric fields, magnetic fields, etc. [10,11]. As a result, propellants using smart materials have the ability to proactively adjust their shapes under different environmental temperatures. Therefore, geometry can be considered as a temporary variable for adjusting burning behavior. In addition, the smart

* Corresponding author.
** Corresponding author.
E-mail addresses: njyangweitao@163.com (W. Yang), zhangxuan@nwpu.edu.cn (X. Zhang).
Peer review under responsibility of China Ordnance Society

https://doi.org/10.1016/j.dt.2023.06.015

propellant can also be judged by human-induced signals.

In this paper, the smart propellant consisting SMPs has been fabricated, and the basic performances and shape memory behaviors are exhibited. The morphology change of fabricated samples has been verified under heat stimuli.

2. Experimental sections

2.1. Raw materials and UV-assisted DIW 3D printing

Kuang X [12] created a shape memory polymer that can be printed using UV-assisted DIW printing. In this study, the raw materials are the listed in Table 1. Polycaprolactone (PCL), EBECRYL®8413 and BA were added to the kneader which was heated by oil of 70 °C for 1 h to melt the PCL particles, then all the materials were mixed in the kneader at 200 r/min for 3 h. The photoinitiator, ethyl (2,4,6-trimethylbenzoyl) phenylphosphinate (TPO-L), was then added and keep stirring for 30 min under vacuum condition to remove the trapped gas in the resins.

Solid filler CL-20 ($d_{50} = 8$ μm) was mixed with the resin matrix in a kneader at 60 °C for 1 h. The resulting propellant formulation contained 70% CL-20. As shown in Fig. 1, the composite slurry was extruded, deposited, and cured using a UV & thermal-assisted DIW printer. The cylinder temperature was maintained at 60 °C and pressure at 0.4 MPa while the deposited strip was cured under UV light with a wavelength of 405 nm.

2.2. Characterization

SMP composite containing CL-20 and SMP polymer shown in Fig. 2 are prepared for shape memory performance test. Dumbbell samples were used in the universal tensile test machine (1036 PC, CN) and the stress-strain curve was obtained at a speed of 100 mm/min at 25 °C. In angle recovery tests, SMP and its energetic composite strips were folded in half or stretched at 70 °C for 2 min and cooled in ice water to fix the shape. The samples were heated again and the shape memory performance was captured by a camera and the reversing time was recorded at various reversing corner. Meanwhile, the stability of the shape memory cycle was also tested. The stretch-recovery cycle begins with the same process as the angle recovery test., and the interval of each cycle is 10 min.

The decomposition behavior of the energetic SMP composites containing CL-20 was measured by a differential scanning calorimeter (DSC, DSC-204, NETZSCH, GER) in a nitrogen atmosphere with a test range of 50–400 °C and a heating rate of 2.5–20 °C/min. The isoconversional model-free modified Kissinger–Akahira–Sunose (KAS) method (see Eq. (1)) is used to obtain the kinetic triplets [13].

$$\ln\left(\frac{\beta}{T_{\alpha,i}^{1.92}}\right) = \text{Const} - 1.0008\frac{E_\alpha}{RT_\alpha} \tag{1}$$

where β is the heating rate, α is the extent of conversion, and T_α is temperature at specific α.

The burning behavior was characterized in a 100 mL closed bomb as shown in Fig. 3. The propellant is ignited by 1.1 g nitrocellulose powder packed in the ignition bag. The size of tested energetic sample is 10 mm × 2 mm × 50 mm. The mass of propellant is 20 g. The pressure history (P/t) was recorded and the burn rate (u-p) curves can be derived as previous methods [14].

Table 1
Properties of materials used in this section.

Reagent	Specification	Mass fraction/%
PCL	MACKLIN®, $M_n = 20{,}000$	26
EB8413	EBECRYL® 8413 (be diluted by IBOA)	37
butyl acrylate (BA)	ALADDIN®, Chemically pure	34
TPO-L	ALADDIN®, Purity 98%	3

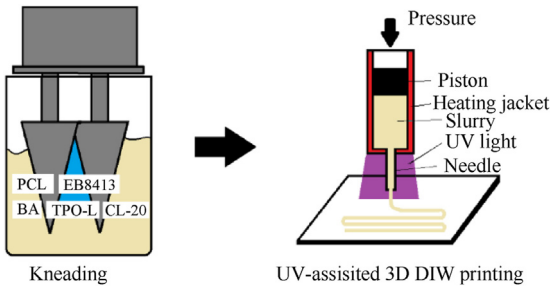

Fig. 1. Schematic illustrations of the UV-assisted DIW-based 3D printing.

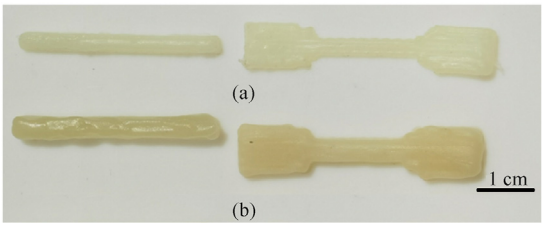

Fig. 2. UV-assisted DIW printed (a) SMP composite samples and (b) pure SMP samples.

3. Results and discussion

3.1. The inner structure and mechanical strength

By utilizing 3D printing technology, we can create and program energetic composite samples as depicted in Fig. 4. Fig. 4 illustrates the transformation of the macromolecule system during the shape-reversing process. During printing, the slurry consisting mainly of oligomers, active diluents (IBOA and BA), initiators, and solid fillers is extruded at 70 °C onto a plate and cured under UV light. After being cured by UV light, the UV resin formed a crosslinked network in which the molten PCL chains interpenetrated and confined in the network. Upon cooling, the PCL chains crystallize and disperse throughout the network. When programming SMP composites, heating, programming, cooling and forming are used to obtain a sample with temporary shape.

The smart material is composed of reversible phase and stationary phase. In this case, PCL chains act as the reversible phase which can melt or crystalize under high or low temperatures. While

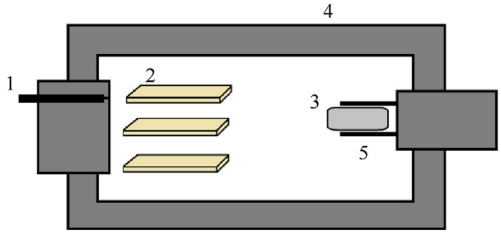

1—Pressure sensor; 2—Tested samples; 3—Ignition bag;
4—Closed bomb; 5—Ignition electrode

Fig. 3. Schematic diagram of closed bomb test.

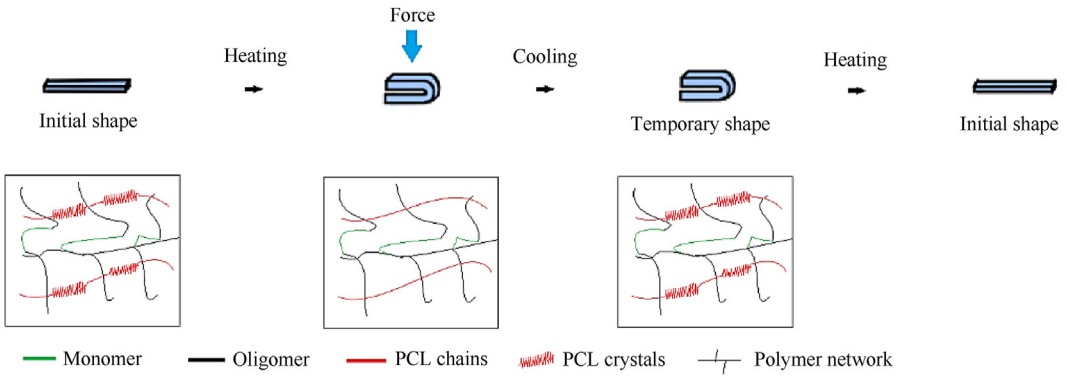

Fig. 4. Schematic illustrations of shape changing and the corresponding inner structure.

the photocured polymer network acts as stationary phase which is responsible for memory and recovery. When heating the sample again, the crystallized PCL melts and becomes soft, and the sample reversed to the initial morphology, due to the internal stress remaining in the crosslinked network.

Fig. 5 displays SEM images of the cross section and tensile curves for both SMP and its composite. In Fig. 5(a), large sphaerocrystals of PCL dispersed in the matrix resins. It is evident that PCL and matrix resins (photocured EB8413 and BA) are incompatible systems, leading to phase separation after PCL crystallization. Additionally, Fig. 5(a) shows that CL-20 particles limit the formation of large sphaerocrystals of PCL. Finally, Fig. 5(b) presents strain-stress curves from a tensile test.

Fig. 5(c) shows a stress-strain curve with two different slopes that reveal the evaluation of crystalline and elastic phases. The ultimate stress and ultimate strain of SMP are 3000 kPa and 235%, respectively. However, when the SMP composite contains 70% CL-20 particles, the ultimate stress and strain decrease to 1300 kPa and 140%, respectively. From the slope of the stress-strain curve, it can be seen that the elastic modulus of the SMP composite (448 kPa) is higher than that of pure SMP without filler (120 kPa) because the CL-20 particles enhance mechanical property of resins.

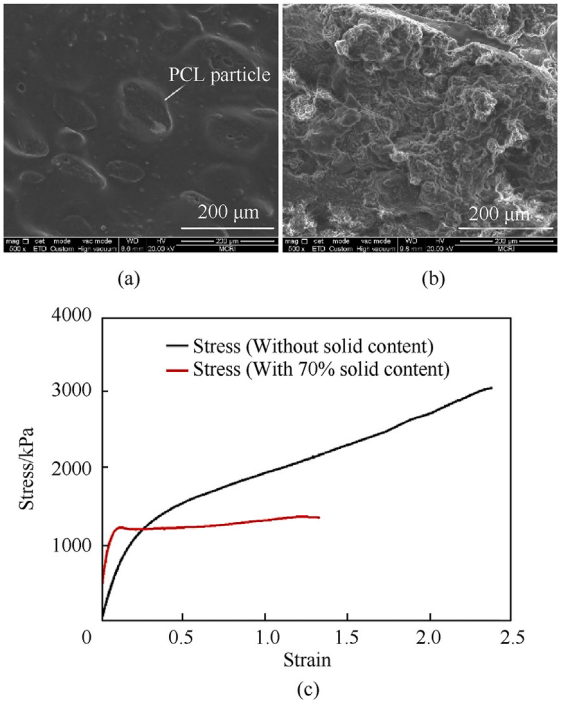

Fig. 5. SEM photo of (a) SMP, (b) SMP composite and (c) strain-stress curves of SMP and its composite containing CL-20.

3.2. The shape memory performance of SMP and its composites

The shape memory performance of SMP and its energetic composites were experimentally demonstrated. Firstly, an angle recovery test was conducted on SMP and SMP energetic composite prepared by 3D printing. The sample sheet was heated in 70 °C water for 2 min, folded in half under external force, and then soaked in 15 °C water for 1 min to fix the temporary shape. When testing the reversing performance, the sample was immersed again in 70 °C water, and the deformation time at a specific angle was recorded. The angle reversing process of the sample under thermal stimulation was shown in Fig. 6.

As depicted in Fig. 6, both SMP and its composite containing 70% solid filler exhibit complete shape recovery upon thermal stimulation, with respective recovery times of 15 s and 18 s. Additionally, it is evident from Fig. 6 that the reversing response rate of the tested sheet containing solid filler is inferior to that of pure SMP due to the restricted mobility of the cross-linked binder system caused by solid fillers impeding the polymer's recovery.

The stability of the shape memory cycle is a crucial factor in assessing the printed SMP and its composites. This cycle begins with the same process as the angle recovery test, wherein the 3D-printed material is immersed in hot water, stretched to near maximum length, and then cooled in cold water. Subsequently, this stretched material is once again soaked in hot water to restore it to its original length. It is important to monitor fixation and recovery times throughout this stretch-recovery cycle. Fig. 7 shows the stretch-time and temperature-time diagram of the 3D-printed SMP and its composite during 10 reciprocating deformation and recovery. As shown in Fig. 7, the original length of the 3D-printed SMP is 1.45 cm, and the maximum length of the first run is 4.35 cm at 70 °C. Thus, the maximum elongation of the first cycle is 300%. It can also be seen that when the temperature rises to 70 °C and falls to 20 °C, in 10 cycles, the maximum elongation is generally about 300% of the original length, and the recovery length is about 110% of the original length. The maximum elongation and the recovered elongation increased slightly after multiple cycles, possibly due to the repeated tensile forces of multiple cycles reducing the friction between the molecular chains. As a results, the mobility of the molecular chain is enhanced, and the molecule is fixed in the deformed chain conformation, providing a higher elongation of nearly 310% for subsequent cycles. The stable extension limit and recovery length demonstrate the high durability of 3D printed materials without solid components.

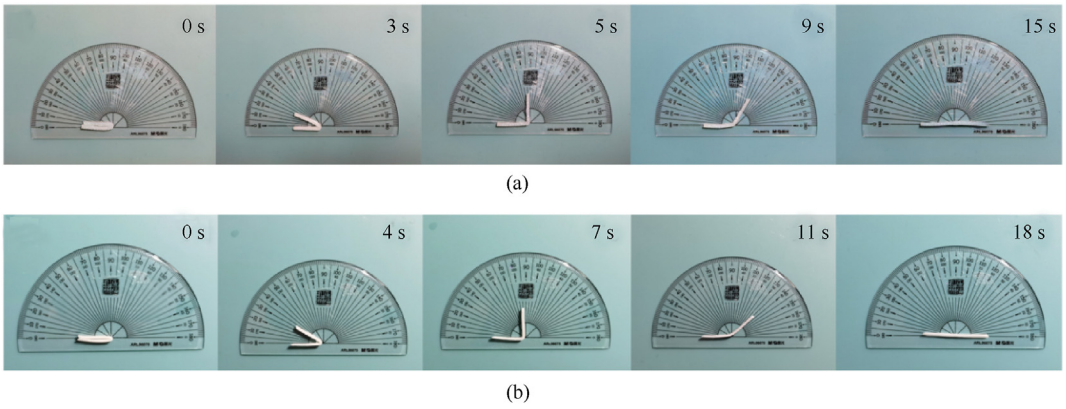

Fig. 6. Angle recovery process of 3D printed SMP: (a) SMP; (b) SMP composite.

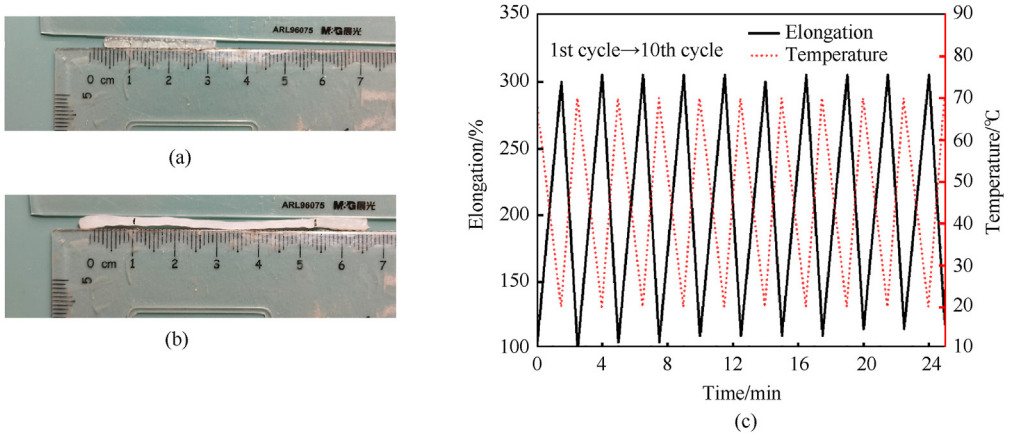

Fig. 7. (a) Photo of 3D printed SMP; (b) Photo of stretched 3D printed SMP; (c) Elongation–time and temperature–time diagrams of cyclic stability test.

The original length of 3D printing material with 70% solid content is 1.05 cm, and the first maximum length is 2.90 cm as shown in Fig. 8(a). Therefore, the maximum elongation of the first cycle is 276%. When the temperature rises to 70 °C and falls to 20 °C, the maximum elongation is generally about 280% of the original length and the recovery length is about 105% of the original length during 10 cycles (shown in Fig. 8(b)). There is also a slight increase in maximum elongation and recovered elongation after multiple cycles, but the effect of higher elongation was negligible. The stable extension limit and recovery length demonstrate that the 3D-printed SMP composite with 70% solid content is also durable.

It can be seen from Figs. 7 and 8 that the average elongation of the filler-free 3D printing SMP is higher than that of 3D-printed SMP composite with solid filler. This is due to the presence of CL-20 particles in the cross-linked system. Solid particles are uniformly distributed around the molecular chain, resulting in greater steric

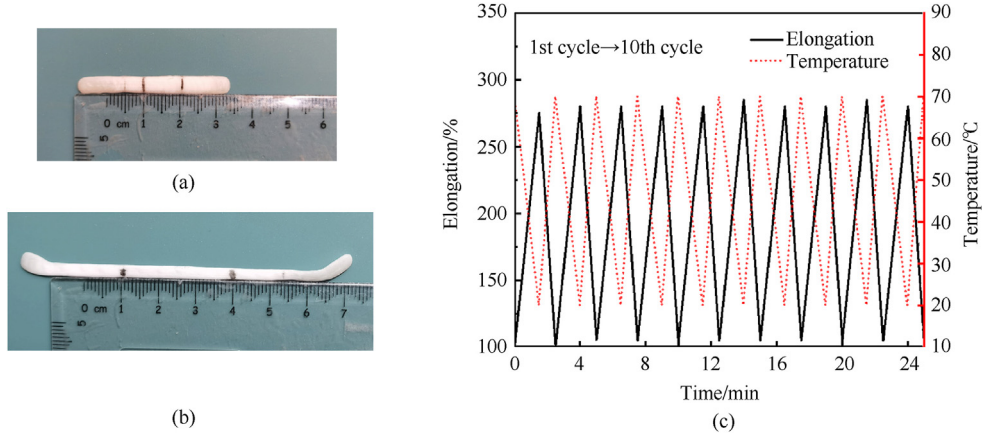

Fig. 8. (a) Photo of 3D printed SMP containing 70% solid; (b) Photo of stretched 3D printed SMP composite; (c) Elongation–time and temperature–time diagrams of cyclic stability test.

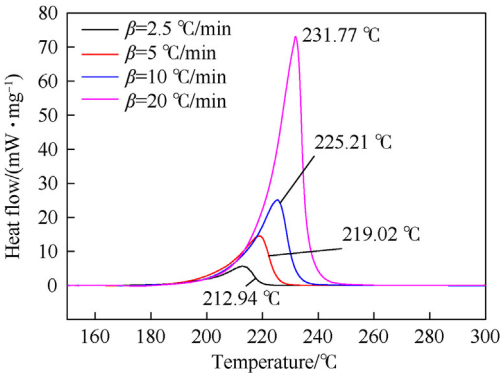

Fig. 9. DSC curves of energetic SMP composite containing CL-20.

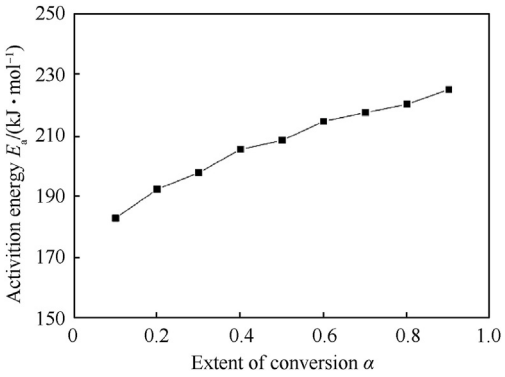

Fig. 11. Dependence of activation energy on extent of conversion of BCHMX/GAP.

hindrance to be overcome during the chain extension and contraction. Therefore, the expansion rate of 3D printed SMP composite is not as good as that of 3D printed SMP.

3.3. Thermal decomposition performance

Fig. 9 presents the DSC curves of energetic SMP composite containing 70% CL-20. As shown in Fig. 9, the peak temperatures increased from 212.94 to 231.77 °C with the increase of the heating rate. Compared with the thermal decomposition of CL-20 in previous studies on thermal decomposition of CL-20 [15,16], it can be found the peak temperatures at the same heating rate was ~30 °C advanced. Foltz et al. [17] found that the phase transition of the β modification began at a temperature of 60 °C, and long-time heating of CL-20-estane-based formulations at 100–105 °C led to $\alpha \rightarrow \gamma$ and $\varepsilon \rightarrow \gamma$ phase transition. In this paper, it is also supposed that crystal transformation of CL-20 particles occurred during the kneading and printing process under heating. By integrating the obtained exothermic peak and then dividing it by the total area, α-T curve shown in Fig. 10 for each exothermic reaction under a certain heating rate can be obtained. The modified KAS method could be used to calculate the kinetic parameters at different extent of conversion α, and the obtained activation energies (E_α) for decompositions of SMP composite containing CL-20 are shown in Fig. 11. The values of kinetic triplets are summarized in Table 2. The mean activity energy calculated by KAS method is 207.03 kJ/mol, which is similar to that of pure CL-20 [18,19].

In the gun field, the pressure rise and burn rate can be measured by the burning of a given weight of propellant in a closed vessel of know volume. In order to evaluate the combustion behavior of SMP-based gun propellants, closed bomb tests were performed.

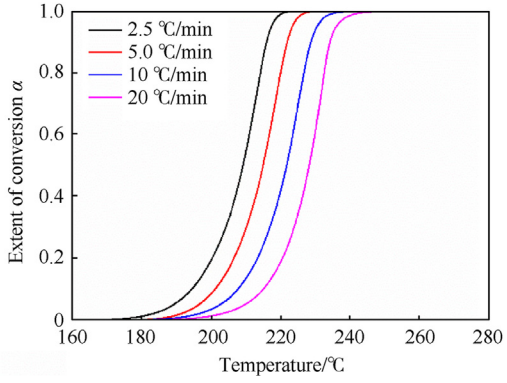

Fig. 10. α-T curve of energetic SMP composite containing CL-20.

Table 2
The kinetic parameters by the modified KAS method from non-isothermal DSC data.

Reacted α	E_α/(kJ·mol^{-1})	R^2	lnA_k/s^{-1}
0.1	182.87	0.9997	52.56
0.2	192.33	0.9995	54.42
0.3	197.68	0.9993	55.40
0.4	205.36	0.9993	57.05
0.5	208.27	0.9994	57.54
0.6	214.46	0.9995	58.91
0.7	217.34	0.9993	59.44
0.8	220.11	0.9992	59.91
0.9	224.82	0.9991	60.91
Mean value	207.03	–	57.35

Fig. 12 presents the P/t and u-p curves of SMP composite containing CL-20. As shown in Fig. 12(a), the burn time and the maximum pressure is 51 ms and 183 MPa, respectively. The burn rate data is obtained from the pressure vs. time data. The burn rate of SMP composite is relatively lower than traditional gun propellants composed of nitrocellulose [20,21], resulting from the inert SMP binder. In general, the combustion rate of gunpowder is an exponential function of ambient pressure. The derived burn rate function from u-p curve in Fig. 12(b) is $u = 0.14\ P^{0.58}$. The burn rate calculations showed a lower pressure exponent than other propellants containing high content of solid filler. The pressure exponent indicates burn rate is less dependent on pressure.

4. Conclusions

In summary, due to the excellent mechanical properties and shape memory performance of printed composite material, 3D printing is an effective method to manufacture smart composite materials with multi-morphologies.

(1) Using PCL as the matrix, butyl acrylate and acrylic cross-linking agent (EB8413) as the reinforcing phase, toluene as the solvent, and CL-20 as the filler. A PCL-poly (butyl acrylate) composite material with good shape memory performance and mechanical properties was fabricated by 3D printing method, which realizes sequential deformation under temperature control.
(2) Both 70% solid content PCL-poly (butyl acrylate) composite material and the unfilled one have good angle recovery and tensile recovery properties. The time need for the two materials that recovery 180° is less than 20 s, and the maximum elongation after ten cycles is still approximately equal to the first elongation, which demonstrates good shape recovery rate and cycle stability of shape memory.

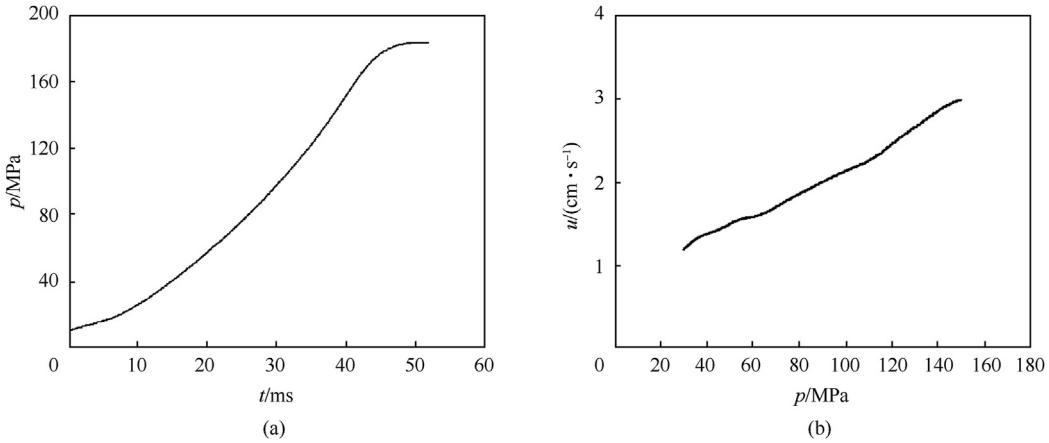

Fig. 12. (a) *p-t* and (b) *u-p* curves of energetic SMP composite containing CL-20.

(3) 3D printing materials with 70% solid content have significant bigger steric hindrance than that of unfilled 3D printing materials due to interaction between solid particles and cross-linking systems. However, the implementation of high solid content printing can give more possibilities to 3D printing materials. For example, when functional materials such as boron nitride are used as fillers, composite materials with good thermal conductivity and shape memory properties can be obtained, providing a material foundation for the design of high-performance shape memory composite materials for 3D printing.

Declaration of competing interest

The authors declare the following financial interests/personal relationships which may be considered as potential competing interests.

References

[1] Gaunce MT, Osborn JR. Temperature sensitivity coefficients of solid propellant burning rate. Acta Astronaut 1986;13(3):127–30.
[2] Cohen NS, Flanigan DA. Mechanisms and models of solid-propellant burn rate temperature sensitivity-A review. AIAA J 1985;23(10):1538–47.
[3] Boulkadid Karim Moulai, Lefebvre Michel, Jeuniea Laurence, Dejeaifve Alain. Influence of firing temperature on properties of gun propellants. J. Chem. Chem. Eng. 2015;9:415–27.
[4] Wang Zeshan, Shi Xianyang. Propelling charges with low temperature sensitivity. Beijing: National Defense Industry Press; 2006.
[5] Li M, Hu R, Gao Y, et al. Combustion behavior of end-sealed nitroamine propellant by photocurable composite deterrents. FirePhysChem 2023;(3):37–42.
[6] Yang W, Hu R, Zheng L, et al. Fabrication and investigation of 3D-printed gun propellants. Mater Des 2020;192:108761.
[7] Li M, Yang W, Xu M, et al. Study of photocurable energetic resin based propellants fabricated by 3D printing. Mater Des 2021;207:109891.
[8] Gao Y, Yang W, Hu R, et al. Validation of CL-20-based propellant formulations for photopolymerization 3D printing. Propellants, Explos Pyrotech 2021;46(12):1844–8.
[9] Wan X, Luo L, Liu Y, et al. Direct ink writing based 4D printing of materials and their applications. Adv Sci 2020;7(16):2001000.
[10] Behl M, Lendlein A. Shape-memory polymers[J]. Mater Today 2007;10(4):20–8.
[11] Lee JY, An J, Chua CK. Fundamentals and applications of 3D printing for novel materials. Appl Mater Today 2017;7:120–33.
[12] Kuang X, Chen K, Dunn CK, et al. 3D printing of highly stretchable, shape-memory, and self-healing elastomer toward novel 4D printing. ACS Appl Mater Interfaces 2018;10(8):7381–8.
[13] Vyazovkin S, Burnham AK, Favergeon L, et al. ICTAC kinetics committee recommendations for analysis of multi-step kinetics. Thermochim Acta 2020;689:22.
[14] Shimpi SA, Krier H. The closed bomb test for the assessment of solid propellant grains utilized in guns. Combust Flame 1975;25:229–40.
[15] Yan Q, Zeman S, Elbeih A, et al. The effect of crystal structure on the thermal reactivity of CL-20 and its C4 bonded explosives (I): thermodynamic properties and decomposition kinetics. J Therm Anal Calorim 2013;112:823–36.
[16] Yan Q, Zeman S, Elbeih A, et al. The influence of the Semtex matrix on the thermal behavior and decomposition kinetics of cyclic nitramines. Cent Eur J Energ Mater 2013;(10):509–28.
[17] Foltz MF, Coon CL, Garcia F, Nichols III AL. The thermal stability of the polymorphs of hexanitrohexaazaisowurtzitane, Part II. Propellants, Explos Pyrotech 1994;19:133–44.
[18] Gołofit T, Zyśk K. Thermal decomposition properties and compatibility of CL-20 with binders HTPB, PBAN, GAP and polyNIMMO. J Therm Anal Calorim 2015;119(3):1931–9.
[19] Zhu YL, Shan MX, Xiao ZX, et al. Kinetics of thermal decomposition of ε-hexanitrohexaazaisowurtzitane by TG-DSC-MS-FTIR. Kor J Chem Eng 2015;32(6):1164–9.
[20] Armstrong RW, Baschung B, Booth DW, et al. Enhanced propellant combustion with nanoparticles. Nano Lett 2003;3(2):253–5.
[21] Courty L, Gillard P, Ehrhardt J, et al. Experimental determination of ignition and combustion characteristics of insensitive gun propellants based on RDX and nitrocellulose. Combust Flame 2021;229:111402.